JACS
JOURNAL OF THE AMERICAN CHEMICAL SOCIETY

Communication

pubs.acs.org/JACS

Crystallographic Dependence of CO Activation on Cobalt Catalysts: HCP versus FCC

Jin-Xun Liu,[‡] Hai-Yan Su,[‡] Da-Peng Sun, Bing-Yan Zhang, and Wei-Xue Li*

State Key Laboratory of Catalysis, Dalian Institute of Chemical Physics , Chinese Academic of Sciences, Dalian 116023, China

Supporting Information

ABSTRACT: Identifying the structure sensitivity of catalysts in reactions, such as Fischer−Tropsch synthesis from CO and H_2 over cobalt catalysts, is an important yet challenging issue in heterogeneous catalysis. Based on a first-principles kinetic study, we find for the first time that CO activation on hexagonal close-packed (HCP) Co not only has much higher intrinsic activity than that of face centered-cubic (FCC) Co but also prefers a different reaction route, i.e., direct dissociation with HCP Co but H-assisted dissociation on the FCC Co. The origin is identified from the formation of various denser yet favorable active sites on HCP Co not available for FCC Co, due to their distinct crystallographic structure and morphology. The great dependence of the activity on the crystallographic structure and morphology of the catalysts revealed here may open a new avenue for better, stable catalysts with maximum mass-specific reactivity.

Identifying the structure sensitivity of catalysts in chemical reactions to achieve the maximum mass-specific yet stable reactivity is one of the most challenging goals in heterogeneous catalysis.[1] A growing number of studies are conducted to understand the nature of the structure sensitivity, supported by well-defined preparation methods, *in situ* characterizations, surface science studies, and *ab initio* calculations. A prime example of this complex structure sensitivity is the Fischer−Tropsch synthesis (FTS) converting CO and H_2 from coal, natural gas, and biomass to hydrocarbon over cobalt catalysts.[2]

Over the years, two notable structure sensitivities have been observed for FTS over Co catalysts, i.e., crystallographic structure and particle size. First, it is noted that Co can exist in two crystallographic structures, namely, the hexagonal close-packed (HCP) phase and the face-centered cubic (FCC) phase, and both phases are found in FTS. It has been reported by many that HCP Co has higher FTS activity than FCC Co.[3] This structure sensitivity is, however, complicated by a phase transition from HCP to FCC upon decreasing the catalyst size,[4] varying the supports and promoters, and pretreating the catalysts.[5] To our best knowledge, it remains open as to whether and why HCP Co catalysts have higher FTS activity than FCC ones, which prevents the full exploration of this structure sensitivity. Second, there are a number of reports on the effect of particle size of Co catalysts on FTS activity; namely, the turnover frequency (TOF) was constant for crystallites above a certain diameter, but when the diameter became smaller, the TOF decreased.[6] It is unclear whether the decrease of FTS activity at the smaller particle size is related to the phase transition of the Co catalyst from HCP to FCC, because of the complexity of the FTS and the absence of sufficient crystallographic structure data. Nevertheless, it is clear that one cannot increase the mass-specific activity of Co catalysts in FTS simply by decreasing the particle size.

We report here a density functional theory (DFT)-based kinetic study (details in Supporting Information) of the effect of the Co crystallographic structures (HCP and FCC) on CO activation, taking into account the influence of hydrogen, because these elementary steps are crucial for the reaction mechanism and the overall reactivity of the FTS. Our calculations show unambiguously that HCP Co has not only a much higher intrinsic activity than FCC Co for CO activation but also a different reaction pathway, i.e., preferentially direct dissociation, versus H-assisted dissociation on FCC Co. The higher intrinsic activity of HCP Co for CO activation is identified from the formation of various favorable active sites not available for FCC Co, due to their different crystallographic symmetries. Moreover, HCP Co has a morphology effect distinct from that of FCC cobalt, allowing HCP Co to expose much denser yet active sites. The great dependence of the catalytic activity on the catalyst's crystallographic structure, and the corresponding morphology that is revealed, may open a new way to design better, stable catalysts with maximum mass-specific reactivity.

HCP and FCC Co have different bulk symmetries and structures, and these are essential for the type of the exposed facets with distinct surface structures and their relative ratio (so-called morphology), which are decisive for the intrinsic activity/selectivity of the individual facets exposed and their contribution to the overall reactivity. To determine the influence of HCP and FCC Co on CO activation without interference from the catalyst supports, the facets exposed and their ratio S_s for large, free particles can be obtained via the Wulff construction based on surface energies E_s. As an approximation, we calculated the surface energy of numerous facets under vacuum condition (Table S1). As shown in Figure 1 and Table 1, the obtained HCP Co morphology contains six different kinds of facets, and the FCC Co morphology contains four different kinds of facets, with very different E_s and S_s values. The distinct morphology between HCP and FCC Co stems from their different point groups. Bulk HCP Co belongs to the D_{3h} point group, and the corresponding morphology is a dihedral-like shape with two close-packed (0001) facets. Despite the very low E_s of 131 meV/Å^2, (0001) covers only 18% of the total surface area exposed. The open

Received: August 17, 2013
Published: October 11, 2013

   dx.doi.org/10.1021/ja408521w | J. Am. Chem. Soc. 2013, 135, 16284−16287

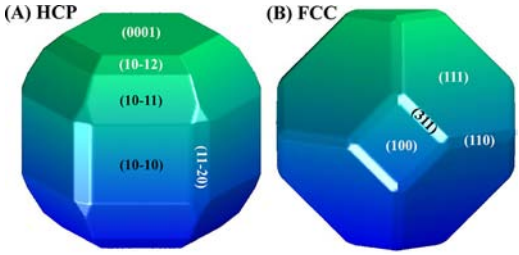

Figure 1. Equilibrium morphology of (A) HCP Co and (B) FCC Co based on the Wulff construction from DFT.

Table 1. Calculated Surface Energies (E_s, in meV/Å^2), Surface Area Proportion S_s (%) of the Various Facets Exposed on HCP and FCC Co from Wulff Construction, and the Corresponding CO Adsorption Energy (E_{ads}), Activation Energy (E_{act}), and Reaction Energy (ΔE) for CO Direct Dissociation (in eV)

facet	E_s	S_s	E_{ads}	E_{act}	ΔE
HCP Co					
(10−11)	149	35	−1.85	1.21	−0.83
(10−10)	140	28	−1.70	1.79	0.46
(0001)	131	18	−1.64	2.46	0.69
(10−12)	156	12	−1.77	1.34	−0.58
(11−20)	155	6	−1.65	1.39	0.32
(11−21)	163	1	−1.82	1.07	−0.05
FCC Co					
(111)	127	70	−1.61	2.48	0.73
(100)	154	12	−1.71	1.49	−0.75
(311)	156	10	−1.71	1.56	−0.18
(110)	151	8	−1.61	1.47	0.39

facets with higher E_s dominate the remaining surfaces, such as (10−11) and (10−12) facets (E_s = 149 and 156 meV/Å^2, S_s = 35% and 12%), (10−10) and (11−20) facets (E_s = 140 and 155 meV/Å, S_s = 28% and 6%), and the (11−21) facet (E_s =163 meV/Å^2, S_s = 1%). On the other hand, FCC Co belongs to the O_h point group with very high symmetry, and the corresponding morphology is an octahedron-like shape, where eight close-packed (111) facets with E_s =127 meV/Å^2 are exposed, covering predominantly 70% of the overall surface area. As a result, the remaining three kinds of open facets, with similar E_s values (∼154 meV/Å^2 on average), cover a relatively smaller portion of the surface area (S_s = 12%, 10% and 8% for (100), (311), and (110), respectively). It is worth noting that the metal−support interaction and metal−reactant/intermediates interaction under operating conditions might affect the corresponding morphology and subsequent reactivity; however, that is beyond the scope of the present work.

We first studied CO adsorption at low coverage on all exposed facets on HCP and FCC Co. The calculated adsorption energies E_{ads} at their most favorable sites (Table S2, Figures S1 and S2) are listed in Table 1. The average value over different HCP Co facets is −1.74 ± 0.088 eV, while on FCC Co it is −1.66 ± 0.058 eV. The average binding on HCP Co is slightly stronger than that on FCC Co. A similar trend was found for atomic H adsorption, and the calculated dissociative adsorption energy varies from −0.47 to −0.58 eV (−0.53 eV on average) for HCP Co and from −0.43 to −0.49 eV (−0.46 eV on average) for FCC Co at the most favorable sites (Table S5). The small difference of CO and H adsorption between HCP and FCC Co, 0.08 and 0.07 eV, clearly reveals a weak crystallographic sensitivity for the adsorption of

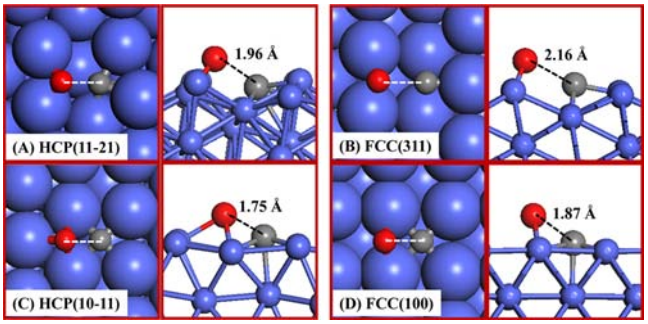

Figure 2. Top and side view of optimized TSs for CO dissociation. Blue, red, and gray balls represent Co, O, and C atoms, respectively.

the reactants involved in FTS. The weak structure sensitivity can also be seen from the small standard deviation of CO adsorption on different facets of HCP Co (±0.088 eV) and FCC Co (±0.058 eV).

CO dissociation in the absence of hydrogen (the so-called direct route) is described here. Taking the favorable CO adsorption sites as the initial state for each exposed HCP and FCC facet allowed the corresponding barriers E_a and reaction energies ΔE to be calculated (Table 1; more details in Table S3, Figures S1 and S2). For close-packed facets, the calculated E_{act} and ΔE are 2.46 and 0.69 eV (endothermic) for HCP (0001), and 2.48 and 0.73 eV for FCC (111). Among all open HCP Co facets exposed, the lowest E_{act} found is 1.07 eV (ΔE = −0.05 eV, exothermic) for the (11−21) faect whereas FCC Co, the lowest E_{act} found is 1.47 eV (ΔE = 0.39 eV) for the (110) facet. This indicates that CO dissociation on both HCP and FCC Co is highly activated and structure sensitive, which agrees well with previous calculations on stepped surfaces.[7] On HCP Co, in addition to the (11−21) facet with the lowest E_{act}, there are other facets, i.e., (10−11), (10−12), and (11−20), also having very low barriers of 1.21, 1.34, and 1.39 eV with favorable ΔE of −0.83, −0.58, and 0.32 eV, respectively. In contrast, for the remaining two FCC Co facets, (100) and (311), the calculated E_{act} values (1.49 and 1.56 eV) are higher than those for the three HCP Co facets mentioned above.

More HCP facets have higher activity of breaking C═O bond than those of FCC due to the formation of the transition state (TS) in HCP. To see this, we first compare two representative TSs, HCP (11−21) (Figure 2A) and FCC (311) (Figure 2B), with a E_{act} difference of 0.49 eV (complete TSs shown in Figures S1 and S2). It can be seen that O fragments locate at 2-fold sites, and no Co atoms are shared by dissociated C and O fragments in both TSs. Thus, the variation in barriers mainly originates from the different locations of the C fragment, the 4-fold-like site for HCP (11−21), and the 3-fold sites for FCC (311). Our calculations show that the 4-fold-like site (−7.30 eV) binds the C fragment at corresponding configurations of the TSs much more strongly than the 3-fold site (−6.52 eV), which can be rationalized as being due to the 4-fold site preference for the C atom on metal surfaces.[8] The large stabilization role of 4-fold sites in C binding can be seen more clearly from two other representative TSs, the HCP (10−11) (Figure 2C) and the FCC (100) (Figure 2D), with a barrier difference of 0.28 eV. In both TSs, C and O fragments share two surface Co atoms, which will raise the overall energetics.[9] However, the binding strengths of the C atom at the 4-fold sites (−8.03 and −7.97 eV for HCP (10−11) and FCC (100) at the TSs) are so strong as to compensate for the energy cost due to the site competition, thus stabilizing

dx.doi.org/10.1021/ja408521w | J. Am. Chem. Soc. 2013, 135, 16284−16287

the corresponding TSs (E_{act} = 1.21 and 1.49 eV). Compared to the TS of FCC (100), where the O fragment occupies a 2-fold site with a binding energy of −5.05 eV, the O fragment with a binding energy of −5.37 eV located at the favorable 3-fold sites for HCP (10−11) provides an additional contribution to its lower barrier. Thus, the flexibility of the formation of the favorable 4-fold site for C and 3-fold site for O on low-symmetry HCP Co is essential to the formation of the favorable active sites with lower CO dissociation barriers.

To quantify the influence of crystallographic phases on the reaction rate r of CO dissociation, a microkinetic model was derived assuming CO adsorption/desorption in equilibrium and irreversible dissociation (details in SI):

$$r = k\theta^*_{CO}\theta^* = kKP_{CO}/(1 + KP_{CO})^2$$

where P_{CO} is the partial pressure of CO, and θ^*_{CO} and θ^* are the coverages of adsorbed CO and the vacant sites, respectively. The rate constant, k, for CO dissociation and the equilibrium constant, K, for CO adsorption were calculated from the above DFT calculation at the low coverage. To be consistent with the low coverage, T = 500 K and $P_{CO} = 3\times10^{-5}$ Pa were used for the rate calculation. We normalized all r by HCP (0001) to facilitate the comparison below.

The calculated reaction rates r for CO dissociation are shown in Figure 3 and detailed in Table S4. For HCP Co (Figure 3A),

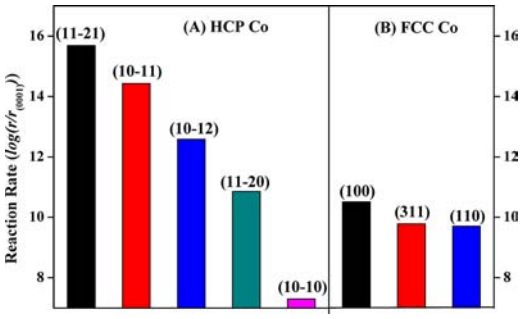

Figure 3. Calculated reaction rates r for CO dissociation on (A) HCP Co and (B) FCC Co at low coverage. All rates are normalized by that of HCP (0001) with units of s^{-1}·site^{-1}.

the HCP (11−21) facet has the highest r, 4.9×10^{15}, among all the facets exposed. It is followed by HCP (10−11), (10−12), (11−20), and (10−10) with values of 2.7×10^{14}, 3.8×10^{12}, 7.2×10^{10}, and 2.0×10^{7}, respectively. The huge r difference between these facets comes mainly from the difference in the CO dissociation barrier. For FCC Co (Figure 3B), r values are calculated to be 3.3×10^{10}, 6.1×10^{9}, 5.1×10^{9} for the (100), (311), and (110) facets, respectively. The smaller r difference between three FCC facets is consistent with their similar dissociation barriers (Table 1).

It can be found from Figure 3 that there are at least four facets, namely, (11−21), (10−11), (10−12), and (11−20) on HCP Co, having reaction rates r higher than that of the most active FCC (100), by a factor of 10^5, 10^4, 10^2, and 2, respectively. This is because all the HCP facets have smaller CO dissociation barriers (Table 1). The fact that HCP Co has a number of distinct facets available with significantly higher reaction rates due to the presence of the more favorable active facets than the most active FCC (100) facet makes the HCP Co a robust catalyst for CO activation. Moreover, the large difference in activity between the different HCP facets implies that, even for the HCP Co catalyst itself, there remains a large freedom to optimize its overall activity by changing its corresponding morphology.

To see this morphology effect more clearly, we note that the previously mentioned four active HCP facets cover more than 50% of the exposed surface area, whereas all three open FCC facets cover only ∼30%, based on the present Wulff construction (Table 1). The larger population of the active HCP Co facets would increase the overall conversion, which further increases the difference in overall activity relative to FCC Co. It is interesting to note that, though the HCP (11−21) facet has the highest reaction rate among all the HCP Co facets exposed (4.9×10^{15}), it covers only 1% of the exposed surface area. While HCP (10−11) also has a relatively higher reaction rate (2.7×10^{14}), it covers 35% of the exposed surface area. Considering the difference in the populations of these two facets, the contribution to the overall activity from HCP (10−11) even surpasses that of HCP (11−21) (Table S4).

These findings are unusual because highly active sites (such as step edges) typically are unstable in nature, and their corresponding concentrations should be low. Exposure of 12 equivalent HCP (10−11) facets covering 35% of the surface area comes from its higher surface atomic density, relative lower surface energy, and HCP Co symmetry. Meanwhile, this facet remains able to form very favorable B5-type sites (Figure 2C). Although the corresponding barrier for CO dissociation is not the lowest among the exposed facets, the calculated value of 1.21 eV is already sufficiently low enough to make HCP (10−11) highly active, considering for instance the FTS typically operating at ∼500 K.

For FTS, the presence of hydrogen may invoke CO activation by the so-called H-assisted route,[10] which could change the above scenario based on the direct route. To see the influence of co-adsorbed atomic H on CO activation, and in particular to get a preliminary understanding of the dependence on the crystallographic phase and orientation of the Co catalysts, the lateral interaction between co-adsorbed CO* and H*, sensitive to the reaction conditions and surface structures, was neglected by placing co-adsorbed CO and H at their most favorable sites with sufficiently large separation. The H-assisted route, CO*+H*→CHO*→CH*+O*, was studied on the most active HCP Co (11−21), (10−11), and (10−12) facets (Table S5, Figures S3 and S4), as well as on all three FCC Co exposed open facets, (110), (311), and (100) (Table S6, Figures S3 and S5). For the direct route calculated above, the corresponding potential energy surfaces were aligned via CO*+H*→C*+O*+H* to facilitate comparison. The calculated overall barriers for the H-assisted route from CO*+H* to CH*+O* on HCP Co (Figure S4) are 1.66, 1.44, and 1.39 eV on (11−21), (10−11), and (10−12), respectively. Compared to the direct route from CO*+H* to C*+O*+H*, with barriers of 1.07, 1.21, and 1.34 eV (Table 1), the H-assisted routes on all three of these HCP facets are kinetically unfavorable. A preference for the direct route for CO dissociation was also found on HCP Ru (11−21) in past work.[10c] For FCC Co (110), (311), and (100) facets (Figure S5), the calculated overall barriers for the H-assisted route are 1.30, 1.36, and 1.52 eV, respectively. Compared to 1.47, 1.56, and 1.49 eV for the direct route (Table 1), the H-assisted route on FCC Co (110) and (311) facets becomes kinetically more favorable, and on FCC (100) it becomes comparable to the direct route.

The overall influence of hydrogen on CO activation described above is best summarized in Figure 4, including various TSs for breaking the C═O bond, with a common zero energy reference of CO+$^1/_2$ H_2 in the gas phase. The distinct preference of a CO

dx.doi.org/10.1021/ja408521w | J. Am. Chem. Soc. 2013, 135, 16284−16287

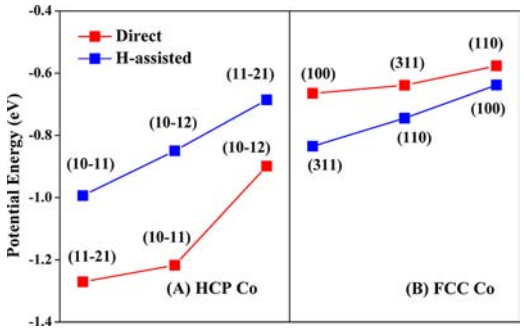

Figure 4. Calculated potential energy (in eV) for CO activation at the transition states for breaking the C═O bond via the direct route (CO*+H*→C*+O*+H*) (red) and the H-assisted route (CO*+H*→CHO*→CH*+O*) (blue) on (A) HCP Co facets and (B) FCC Co facets. The zero energy reference is CO+$^1/_2$ H_2 in the gas phase.

activation reaction pathway, i.e., the direct route for HCP Co and the H-assisted route for FCC Co, is clearly seen. This could be rationalized by the higher activity of the HCP Co for the direct route leaving little room for the H-assisted route. More importantly, Figure 4 shows that the potential energy of the TSs for the direct route on HCP Co is still lower than that of the H-assisted one on FCC Co. In other words, even considering the presence of hydrogen, HCP Co remains more active than FCC Co for CO activation.

The identification of higher intrinsic activity, denser active sites, and stronger morphology effect of HCP Co compared to FCC Co would be valuable for developing more efficient and stable Co catalysts with higher mass-specific reactivity for catalytic reactions related to CO activation, such as methanation and FTS. Since a simple decrease in particle size of more active HCP Co could be accompanied by a phase transformation to less active FCC Co, one could resort to morphology control by exposing large active surface facets, for instance, HCP (10−11), to increase the mass-specific activity of HCP Co catalysts. Thanks to the progress of material synthesis, uniquely faceted yet stable HCP ruthenium nanocrystals with a well-defined hourglass shape, exposing exclusively the (10−11) facet, were reported recently.[11] It would be highly valuable to synthesize HCP Co in this morphology for higher mass-specific reactivity. In this context, we note that the influence of crystallographic structure may be dependent on both the reactant and the metal. For example, it was found that FCC Ru catalysts were more catalytically active for CO oxidation than HCP Ru catalysts.[12]

In summary, we identify theoretically that, for CO activation in the presence of hydrogen, HCP Co catalysts have remarkably higher intrinsic activity than FCC Co catalysts, and HCP Co catalysts prefer the direct dissociation route while FCC Co catalysts prefer the H-assisted route. The great influence of crystallographic structure and corresponding morphology effect on formation of the various active sites with higher intrinsic activity and density is illustrated. The insights revealed might open up a new avenue for the design of better, stable catalysts with maximum mass-specific reactivity, in which *ab initio* calculation and material synthesis would play an essential role.

■ ASSOCIATED CONTENT

Ⓢ Supporting Information

Computations, Figures S1−S5, and Tables S1−S6. This material is available free of charge via the Internet at http://pubs.acs.org.

■ AUTHOR INFORMATION

Corresponding Author

wxli@dicp.ac.cn

Author Contributions

‡J.-X.L. and H.-Y.S. contributed equally.

Notes

The authors declare no competing financial interest.

■ ACKNOWLEDGMENTS

This work was supported by the NSFC (20923001, 21173210, 21225315, 21273224) and 973 Program (2013CB834603). Calculations were carried out at National Supercomputing Center "Tianhe-I" in Tianjin. We thank Prof. D. Ma and Y. J. Ding for fruitful discussions and E. Sanderson for reading the manuscript.

■ REFERENCES

(1) Van Santen, R. A. *Acc. Chem. Res.* **2009**, *42*, 57.

(2) (a) Fu, L.; Bartholomew, C. H. *J. Catal.* **1985**, *92*, 376. (b) Zhao, Y.-H.; Sun, K.; Ma, X.; Liu, J.; Sun, D.; Su, H.-Y.; Li, W.-X. *Angew. Chem., Int. Ed.* **2011**, *50*, 5335. (c) Wang, H.; Zhou, W.; Liu, J.-X.; Si, R.; Sun, G.; Zhong, M.-Q.; Su, H.-Y.; Zhao, H.-B.; Rodriguez, J. A.; Pennycook, S. J.; Idrobo, J.-C.; Li, W.-X.; Kou, Y.; Ma, D. *J. Am. Chem. Soc.* **2013**, *135*, 4149. (d) Fischer, N.; van Steen, E.; Claeys, M. *J. Catal.* **2013**, *299*, 67.

(3) (a) Ducreux, O.; Lynch, J.; Rebours, B.; Roy, M.; Chaumette, P. *Stud. Surf. Sci. Catal.* **1998**, *119*, 125. (b) Enache, D. I.; Rebours, B.; Roy-Auberger, M.; Revel, R. *J. Catal.* **2002**, *205*, 346. (c) de la Peña O'Shea, V. A.; Homs, N.; Fierro, J. L. G.; Ramírez de la Piscina, P. *Catal. Today* **2006**, *114*, 422. (d) Ducreux, O.; Rebours, B.; Lynch, J.; Roy-Auberger, M.; Bazin, D. *Oil Gas Sci. Technol.—Rev. IFP* **2008**, *64*, 49. (e) Karaca, H.; Safonova, O. V.; Chambrey, S.; Fongarland, P.; Roussel, P.; Griboval-Constant, A.; Lacroix, M.; Khodakov, A. Y. *J. Catal.* **2011**, *277*, 14. (f) Gnanamani, M. K.; Jacobs, G.; Shafer, W. D.; Davis, B. H. *Catal. Today* **2013**, *215*, 13.

(4) Kitakami, O.; Sato, H.; Shimada, Y.; Sato, F.; Tanaka, M. *Phys. Rev. B* **1997**, *56*, 13849.

(5) (a) Fischer, N.; van Steen, E.; Claeys, M. *Catal. Today* **2011**, *171*, 174. (b) Braconnier, L.; Landrivon, E.; Clémençon, I.; Legens, C.; Diehl, F.; Schuurman, Y. *Catal. Today* **2013**, *215*, 18. (c) Prieto, G.; Concepción, P.; Murciano, R.; Martínez, A. *J. Catal.* **2013**, *302*, 37.

(6) (a) Bezemer, G. L.; Bitter, J. H.; Kuipers, H. P.; Oosterbeek, H.; Holewijn, J. E.; Xu, X.; Kapteijn, F.; van Dillen, A. J.; de Jong, K. P. *J. Am. Chem. Soc.* **2006**, *128*, 3956. (b) Borg, O.; Dietzel, P.; Spjelkavik, A.; Tveten, E.; Walmsley, J.; Diplas, S.; Eri, S.; Holmen, A.; Rytter, E. *J. Catal.* **2008**, *259*, 161. (c) Den Breejen, J.; Radstake, P.; Bezemer, G.; Bitter, J.; Froseth, V.; Holmen, A.; Jong, K. P. *J. Am. Chem. Soc.* **2009**, *131*, 7197. (d) Herranz, T.; Deng, X.; Cabot, A.; Guo, J.; Salmeron, M. *J. Phys. Chem. B* **2009**, *113*, 10721. (e) Prieto, G.; Martínez, A.; Concepción, P.; Moreno-Tost, R. *J. Catal.* **2009**, *266*, 129. (f) Tuxen, A.; Carenco, S.; Chintapalli, M.; Chuang, C.-H.; Escudero, C.; Pach, E.; Jiang, P.; Borondics, F.; Beberwyck, B.; Alivisatos, A. P.; Thornton, G.; Pong, W.-F.; Guo, J.; Perez, R.; Besenbacher, F.; Salmeron, M. *J. Am. Chem. Soc.* **2013**, *135*, 2273.

(7) Gong, X. Q.; Raval, R.; Hu, P. *Surf. Sci.* **2004**, *562*, 247.

(8) Zhang, C.; Hu, P. *J. Chem. Phys.* **2002**, *116*, 322.

(9) Bleakley, K.; Hu, P. *J. Am. Chem. Soc.* **1999**, *121*, 7644.

(10) (a) Huo, C.-F.; Li, Y.-W.; Wang, J.; Jiao, H. *J. Phys. Chem. C* **2008**, *112*, 14108. (b) Inderwildi, O. R.; Jenkins, S. J.; King, D. A. *J. Phys. Chem. C* **2008**, *112*, 1305. (c) Shetty, S.; Jansen, A. P. J.; van Santen, R. A. *J. Am. Chem. Soc.* **2009**, *131*, 12874. (d) Ojeda, M.; Nabar, R.; Nilekar, A. U.; Ishikawa, A.; Mavrikakis, M.; Iglesia, E. *J. Catal.* **2010**, *272*, 287.

(11) Watt, J.; Yu, C.; Chang, S. L. Y.; Cheong, S.; Tilley, R. D. *J. Am. Chem. Soc.* **2012**, *135*, 606.

(12) Kusada, K.; Kobayashi, H.; Yamamoto, T.; Matsumura, S.; Sumi, N.; Sato, K.; Nagaoka, K.; Kubota, Y.; Kitagawa, H. *J. Am. Chem. Soc.* **2013**, *135*, 5493.